Title

Selective damage sensing in multiscale hierarchical composites by tailoring the location of carbon nanotubes

Journal

Journal of Intelligent Material Systems and Structures, 29(4)

ISSN

1045-389X

Authors

de Jesús Ku-Herrera, José
La Saponara, Valeria
Avilés, Francis

Publication Date

2018-03-01

DOI

10.1177/1045389x17711790

Peer reviewed

Selective damage sensing in multiscale hierarchical composites by tailoring the location of carbon nanotubes

J.J. Ku-Herrera[a*], V. La Saponara[b], F. Avilés[c+]

[a]CONACYT-Centro de Investigación en Química Aplicada. Departamento de Síntesis de Polímeros. Blvd. Enrique Reyna Hermosillo No. 140. San José de los Cerritos. C.P. 25294 Saltillo, Coahuila, Mexico.

[b]University of California Davis, Department of Mechanical and Aerospace Engineering, One Shields Ave, Davis, CA 95616, USA.

[c]Centro de Investigación Científica de Yucatán A.C., Unidad de Materiales, Calle 43 No.130 x 32 y 34, Col. Chuburná de Hidalgo. C.P. 97205, Mérida, Yucatán, Mexico.

Abstract

The selectivity in composite damage sensing using the electrical resistance approach is investigated by deliberately placing multiwall carbon nanotubes (MWCNTs) dispersed within the matrix or deposited onto the fiber surface. To this aim, unidirectional glass fiber/carbon nanotube/vinyl ester specimens with fibers oriented along (0°) and transverse (90°) to the loading direction are subjected to quasi-static tension up to failure. The electrical resistance changes in the composite are correlated to the mechanical strain and acoustic emission events. By using this approach, it is shown that the electrical signal is able to discern between fiber and matrix (or fiber/matrix interface) damage. The electrical resistance of composites with MWCNTs located within the matrix is capable of tracking matrix dominated damage but is poorly sensitive to fiber breakage. In contrast, the composites with MWCNT-modified fibers exhibit outstanding sensitivity to fiber- and fiber/matrix interface damage.

Keywords: Carbon nanotubes; Glass fibers; Hierarchical composites; Structural Health Monitoring; Non-destructive testing

Corresponding authors: faviles@cicy.mx (F. Avilés[+]), Tel: +52 (999) 9438330 Ext. 388

jesus.ku@ciqa.edu.mx (J.J. Ku-Herrera[*]), Tel: +52 (844) 4389830 Ext. 1055

1. Introduction

Fiber-reinforced polymer composites (FRPCs) used for structural applications are designed to retain structural integrity and remain safe for the intended service life (Irving and Soutis, 2014). However, their structural integrity can be compromised given the loading conditions that they are subjected to in service and their complex damage modes. Therefore, it is imperative to develop robust structural health monitoring (SHM) techniques that can provide insightful and real time information about the structural status of the composite to prevent catastrophic failures (Diamanti and Soutis, 2010). Most conventional non-destructive evaluation methods such as eddy currents, C-scan, X-ray radiography, and thermography, may not be suitable for on-line SHM since they may require removal from service for damage inspections (Diamanti and Soutis, 2010; Balageas et al., 2006). Other techniques, such as fiber Bragg grating and piezoelectric-based sensing (such as acoustic emission (AE)) require mounting external several sensors or are susceptible to noise (Farrar and Worden, 2007; Diamanti and Soutis, 2010; Chia Chen et al., 2008). For carbon fiber-reinforced polymer composites, SHM based on electrical resistance measurements, which takes advantage of the inherent conductivity of carbon fibers, has been long explored (Schulte and Baron, 1989; Xiaojun and Chung, 1997; Kostopoulos et al., 2009). The changes in electrical resistance of these carbon fiber composites allow to monitor fiber-dominated damage but are not sensitive to matrix damage (Xiaojun and Chung, 1997; Xiaojun and Chung, 1996; Wang et al., 1999; Wang and Chung, 1998). With advances in nanotechnology, the electrical resistance approach has been recently extended to FRPCs with insulating fibers, by dispersing small amounts of CNTs into the matrix (typically <0.5 wt. %) (Thostenson and Chou, 2008; Gao et al., 2009a; Gao et al., 2009b; Friedrich et al., 2011; Fernberg et al., 2009) or placing/growing them onto fibers (An et al., 2013; Zhang et al., 2010; Sebastian et al., 2014; Gallo and Thostenson, 2015; Wiegand and Mäder, 2016; Hao et al., 2016; Gao et al., 2010; Zhang et al., 2015a; Zhang et al., 2015b). It has been proved that, when percolated into the matrix, CNTs form an electrically conductive network, which is sensitive to strain and composite damage (Thostenson and Chou, 2008; Gao et al., 2009a). This composite architecture has proved good sensing capabilities to monitor matrix-dominated damage. However, very few works have explored the electrical sensing capabilities of glass fibers covered with CNTs (using an unmodified polymer matrix) to monitor damage in polymer composites (An

et al., 2013; Zhang et al., 2010; Gao et al., 2010; Sebastian et al., 2014; Gallo and Thostenson, 2015; Wiegand and Mäder, 2016; Hao et al., 2016). Since most of the works that use CNT-modified glass fibers for damage sensing were conducted on model composites comprising an individual fiber embedded within the matrix, the role the fiber-to fiber interactions on the electromechanical response has been downplayed. Furthermore, a direct comparison of the self-sensing capabilities of glass fiber/CNT/polymer composites with CNT network locations deliberatively placed within the matrix or on the fiber, to detect specific damage mechanisms using the electrical resistance approach has not been addressed. Given this motivation, this work investigates the electrical sensing capabilities of multiwall carbon nanotube (MWCNT)/glass fiber/vinyl ester composites with a tailored-located MWCNT network to self-sense composite damage under tensile loading. To tailor the electrical sensitivity of the composite, the composites are manufactured into two hierarchical architectures distinguished by the location of the MWCNTs, *viz.* with MWCNTs randomly dispersed within the matrix and with MWCNTs deposited onto the glass fibers previous to composite manufacturing. To prove the selectivity concept in the electrical signal, unidirectional 0° and 90° composites with well-known failure modes are used as model materials, and their mechanical response upon tensile loading is correlated to the changes of electrical resistance and AE events.

2. Materials and methods

2.1. *Materials*

Commercial MWCNTs (Cheap Tubes Inc., Vermont, USA) with purity >95%, 30-50 nm outer diameter, 5-10 nm inner diameter, and 1-6 μm length were used. All MWCNTs were chemically oxidized using a solution of H_2SO_4/NHO_3 at 3 M, for 2 h following the procedure described in (Avilés et al., 2009). Continuous E-glass fibers (Poliformas Plásticas S.A de C.V., Mérida, Mexico) with an average diameter of 15 μm, density of 2.54 g/cm^3 in the form of fiber tows containing ~4000 filaments/tow were used. An epoxy vinyl ester Hetron 992 FR resin from Ashland composites (Dublin, OH, USA) was used as polymer matrix. Cobalt naphthenate (CoNap) in a proportion of 0.2 wt. %, and 0.6 wt. % of methyl ethyl ketone peroxide (MEKP) were used to manufacture the multiscale composites.

2.2. *Manufacturing of hierarchical composites*

In order to tailor the electrical sensitivity of the composites to detect specific damage mechanisms, the MWCNT network inside the composite was deliberately built into two hierarchical architectures, differentiated by the location of the MWCNTs (see Fig. 1). The first architecture (Fig. 1a, architecture "*m*"), comprises of MWCNTs randomly dispersed within the matrix, while for the second one (Fig. 1b, architecture "*f*") MWCNTs were previously bonded to the fiber. The deposition of MWCNTs onto the glass fibers was conducted following the dipping procedure reported in our previous works (Ku-Herrera et al., 2015; Ku-Herrera et al., 2014). Briefly, MWCNTs were first dispersed in distilled water using an ultrasonic bath; then the glass fiber tows were immersed into the MWCNT/water suspension and the MWCNT deposited following ultrasonic agitation. Chemical interactions between the oxidized MWCNTs and the fiber surface coating (sizing) allowed bonding of the MWCNTs to the fiber surface (Ku-Herrera et al., 2015).

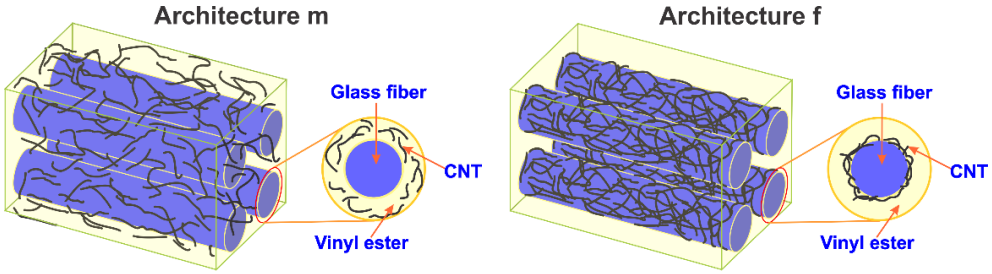

a) b)

Figure 1. Schematic of the multiscale hierarchical composite architectures. a) Architecture *m*, with MWCNTs dispersed in the matrix, b) architecture *f*, with MWCNTs bonded to the fibers.

Unidirectional composite laminates with fibers oriented at 0° and 90° with respect to the loading direction have well-recognized failure modes under tensile loading and were thus selected as model materials for this work. All composite laminates were manufactured by vacuum assisted resin transfer molding. The laminate layup consisted of three layers of 14 cm long glass fibers. For the composite architecture *f*, the preform was made using MWCNT-modified glass fibers and unmodified vinyl ester resin was infused. For composites with architecture *m*, the preform was made of as-received glass fibers, and a modified vinyl ester resin containing randomly dispersed MWCNTs was used to impregnate the fiber preform. Such a MWCNT-modified matrix was achieved by mixing 0.5 wt. % MWCNTs (with respect to the weight of the resin and

nanotubes) with the vinyl ester resin assisted by ultrasound (70 W, 42 kHz, for 3 h), prior to infusion. This MWCNT weight content was selected for being slightly above the electrical percolation threshold (~0.2 wt. %) of the MWNCT/vinyl system, as discussed in our previous work (Ku-Herrera et al., 2013). Concentrations closer to the electrical percolation yield issues related to instrumentation when measuring such high electrical resistances, and thus were not used. Regarding the glass fiber content, both composite architectures have a fiber volume fraction of 0.48, measured by resin burn-off following the procedure recommended by the ASTM standard D2584 (ASTM-International, 2011). By considering the weight fraction of the glass fibers (~0.73) and the resin (~0.27) within the composites, measured during the resin burn-off experiment, the estimated MWCNT content for the composites with architecture *m* is ~0.14 wt. %. For the composite with architecture *f,* according to previous research the upper bound content of MWCNT deposited on the glass fibers is 0.5 wt. % (with respect to the glass fiber weight) (Ku-Herrera et al., 2015). Using this assumption, the upper bound of the MWCNT content in the hierarchical composite with architecture *f* is estimated as 0.36 wt. %. In order to promote uniform electrical contact among fibers for the composite architecture *f*, a conductive 0.5 wt. % MWCNT/vinyl ester mixture was applied at the ends of the fiber preform (i.e. at the tabbed region), to define electrical contacts. All laminates were allowed to cure at room temperature for 2 h and then postcured using a convection oven for 4 h at 82 ºC.

2.3. *Tensile test setup*

The selectivity of both composite architectures (*f* and *m*) to detect damage at the matrix, fiber, and fiber/matrix interface levels was evaluated by subjecting the 0° and 90° unidirectional specimens to a monotonic uniaxial tensile loading up to failure. The specimen preparation for the electro-mechanical characterization consisted in end-tabbing the laminates, bonding strain gages and electrodes instrumentation. Schematics of the 0° and 90° instrumented specimens are shown in Fig. 2. For the composites with fibers aligned along the load direction (0° specimens), 25 mm long tabs made of plain weave glass fibers/vinyl ester were adhesively bonded at the ends of the laminate, while 20 mm long tabs were used for the 90 °specimens (with fibers aligned perpendicularly to the loading direction). Both tensile specimens (0° and 90°) were obtained by cutting the composite laminates with dimensions scaled down (1:2 ratio) from the dimensions recommended by the ASTM standard D3039 (ASTM-International, 2014). The 0° specimens

were 120 mm long and 7 mm wide, with a nominal thickness of 1.0 mm defined by the three layers employed. Likewise, the 90° specimens were 90 mm long, 12 mm wide and ~1.0 mm thick. Silver paint strips was applied at the edges of the specimens, close to the end tabs to bond a couple of copper wires as electrodes, as indicated in Fig. 2. The electrical resistance of the specimens was measured before tensile testing to obtain the electrical resistance at zero load/strain, named R_0. The two-point probe method was used for the electrical resistance measurements, as suggested for samples with high electrical resistance (MacInnes, 1992); this is because the electrical resistance of the specimens tested was in the order of MΩ, which is several orders of magnitude higher than their contact resistance (~Ω). A Shimadzu AG-I universal testing machine was employed to apply the tensile loading at 1 mm/min crosshead displacement rate. For the 0° specimens a 20 kN load cell was used as force sensor, while a 500 N load cell was used for the 90° specimens. Strain was recorded by means of unidirectional strain gages (350 Ω, gage factor of 2.125) using a Vishay P3 strain indicator. The change in electrical resistance (ΔR) of the specimen was measured during testing using an Agilent DMM 3441 digital multimeter, synchronizing all instruments using an in-house data acquisition software. For the AE analysis, two PICO-type piezoelectric transducers were attached at the center of the specimen surface, 40 mm apart (Fig. 2). The data acquisition system for the acoustic emissions was a PCI-2-based AE system (Physical acoustic, Princeton Junction, NJ, USA). Acoustic emission signals were amplified using a preamplifier with a gain of 40 dB and band pass-filtered for 20-1200 kHz. A threshold of 40 dB was used to filter-out the noise not related to the acoustic events within the composite. Additionally, all acoustic events not coming from the gap between the sensors were discarded. Five replicates of the 0° and 90° specimens for each composite architecture were tested up to fracture. The axial stress (σ_1 or σ_2, being "1" the conventional fiber direction, and "2" the in-plane transverse one), strain (ε_1 or ε_2), the electrical resistance (R) and the acoustic events occurring during tensile testing were acquired simultaneously.

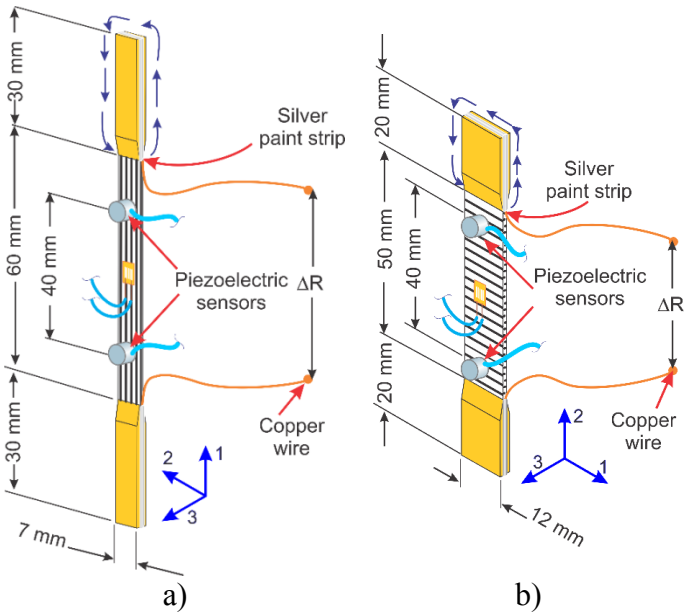

Figure 2. Specimen dimensions and instrumentation. a) 0° specimen, b) 90° specimen.

3. Results

3.1. *Damage sensing for 90 ° specimens*

The electrical sensitivity of both composites ("*f*" and "*m*") to monitor their tensile damage until fracture was first studied using specimens with fibers oriented 90° with respect to the loading direction. For the composite with hierarchical architecture *m*, Fig. 3a shows the stress (σ_2), the electrical signal ($\Delta R/R_0$), and the amplitude of the recorded acoustic events as function of the strain (ε_2). Cumulative energy (in zJ=1x10^{-21} J) of the acoustic events showed in Fig. 3a are then plotted in Fig. 3b as function of ε_2. Figure 3c shows scanning electron microscope (SEM) images of the fractured surface of the 90° specimen for composite architecture *m*. Notice in Fig. 3c (bottom) that MWCNTs are indeed protruding from the matrix, confirming that the intended architecture was achieved. As seen in Figs. 3a and 3b, acoustic events are not detected for $\varepsilon_2 <$ 0.1%, indicating that the composite deformed elastically without evident damage at such a strain level, and thus the electromechanical response is attributed solely to piezoresistivity. Thereafter, few acoustic events exhibiting amplitudes around 40-70 dB, with frequencies ranging from 90 kHz to 350 kHz (frequencies not shown in the plot) are detected. Those acoustic features are associated to matrix cracking (40-60 dB) and fiber/matrix interfacial damage (60-70 dB) (Masmoudi et al., 2014; Marec et al., 2008). Notice in Fig. 3 the absence of acoustic events with

amplitudes >70 dB, which are associated to fiber breakage (Masmoudi et al., 2014; Marec et al., 2008; Godin et al., 2004; Ativitavas et al., 2004). This indicates that damage of the composite starts by matrix cracking followed by fiber/matrix debonding, which induces the specimen failure. This is confirmed by the SEM images showed in Fig. 3c, where fiber imprints in the matrix are observed, supporting that fiber/matrix debonding is the failure-dominated mechanism in the composite. Likewise, the concomitant $\Delta R/R_0$ response does not present abrupt changes either (which are normally associated to fiber breakage); a slight deviation from linearity in Fig. 3b is observed in the $\Delta R/R_0$ vs. ε_2 curve at $\varepsilon \approx 0.1$ % (indicated by the coefficient of determination r^2=0.996, calculated at $0 \leq \varepsilon_2 \leq 0.1$ %), which coincide with the first acoustic events detected, capturing the onset of composite damage. As seen from the correlation between acoustic emission signals and $\Delta R/R_0$, for this composite architecture (m), the small change in slope of the $\Delta R/R_0$ vs. ε_2 curve can be associated to damage occurring in the matrix, which disrupts the existing MWCNT conductive pathways.

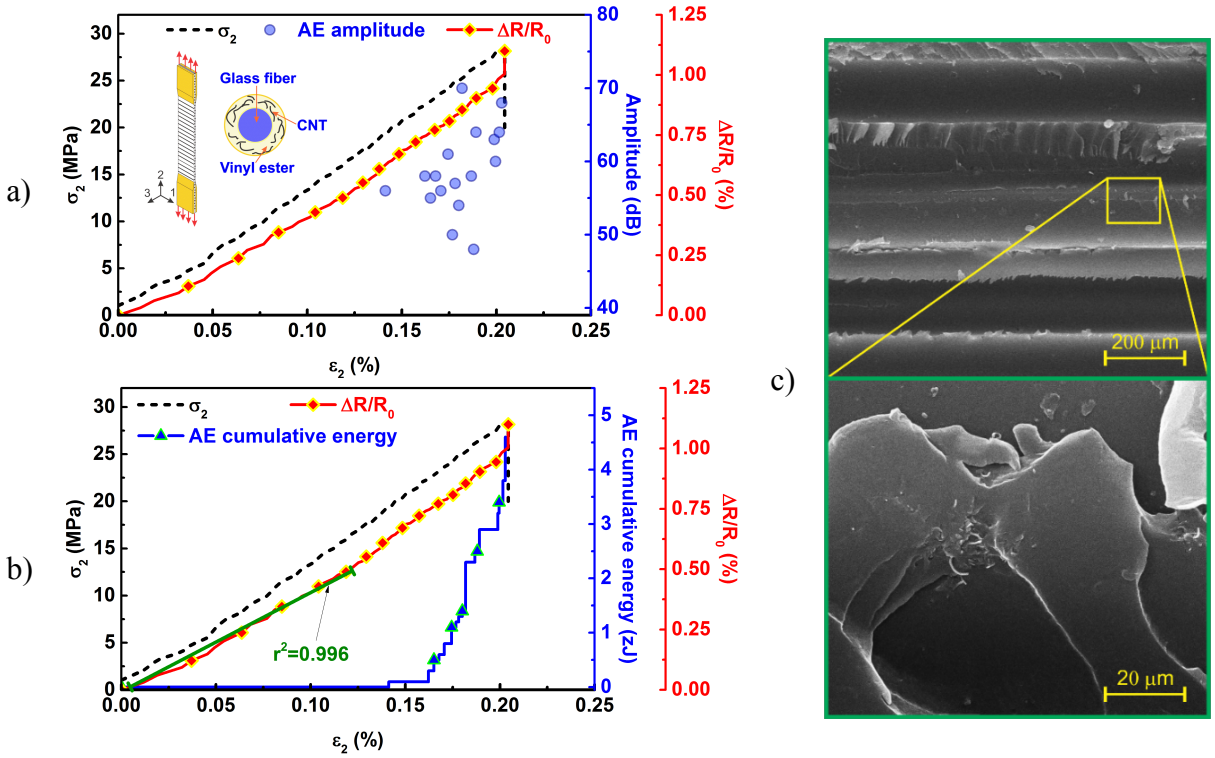

Figure 3. Mechanical, electromechanical, and acoustic emission characterizations of the 90° composites with hierarchical architecture m. a) σ_2 (dashed line), $\Delta R/R_0$ (diamonds), AE

amplitude (scattered circles) plotted against applied strain (ε_2), b) AE cumulative energy (triangles) as function of ε_2, c) SEM image of fractured surface.

Figure 4 shows the electromechanical characterization coupled with acoustic emission of a 90° specimen with hierarchical architecture *f*. Similar to the 90° composite with architecture *m*, the composite with architecture *f* does not exhibit acoustic events for low levels of strain ($\varepsilon_2 < 0.1\%$, Figs. 4a and 4b), suggesting that at such a level of strain, the measured $\Delta R/R_0$ is due to piezoresistivity. By comparing Figs. 3 and 4 at the same level of strain ($\varepsilon_2 < 0.1\%$) is seen that the composite with architecture *f* exhibits higher $\Delta R/R_0\varepsilon_2$ ratio than the composite with architecture *m*. The higher strain sensitivity of the composite with architecture *f* is attributed to the increasing distance among adjacent fibers when they are loaded transversally, which may not be as relevant for $\Delta R/R_0$ when the MWCNT electrical network is located within the matrix. The $\Delta R/R_0$ signal linearly ($r^2 = 0.994$) increases with ε_2 up to $\varepsilon_2 = 0.1\%$, where a change in slope is observed. As for the composite with architecture *m*, the change in slope of the $\Delta R/R_0$ vs. ε_2 curve coincides with the onset of matrix cracking and fiber/matrix debonding, indicated by the acoustic events in Fig. 4a. Notice that the composite with architecture *f* (Fig.4) exhibits a more marked change in the $\Delta R/R_0$ vs. ε_2 slope than that of the composite with architecture *m* (Fig. 3) at this level of strain, suggesting more sensitivity to the onset of this kind of damage. In Fig. 4c the fractured surface also presents fiber imprints in the fractured matrix indicating that fiber/matrix debonding is the failure-dominated mechanism of the composite. Notice also in Fig. 4c (bottom) the presence of MWCNTs on the fibers, which confirms that the tailored architecture *f* was successfully achieved. Regarding the electromechanical response, the load/strain transferred from the matrix to the fibers deforms the electrically conductive CNT network at the fibers surface, which is reflected at the macroscale level by changes in the electrical resistance of the specimens. When growing cracks reach the MWCNT network at the fiber/matrix interface, they destroy effective conductive pathways, yielding a more pronounced increase in the electrical resistance of the composite. Once again the change in slope of the $\Delta R/R_0$ vs. ε_2 curve coincides with the onset of matrix cracking and subsequent fiber/matrix debonding detected by AE, and exhibits a strong correlation between the acoustic events and the changes in electrical resistance. This deviation from linearity may be used to adopt opportune actions to prevent failure of the composite in real-life situations.

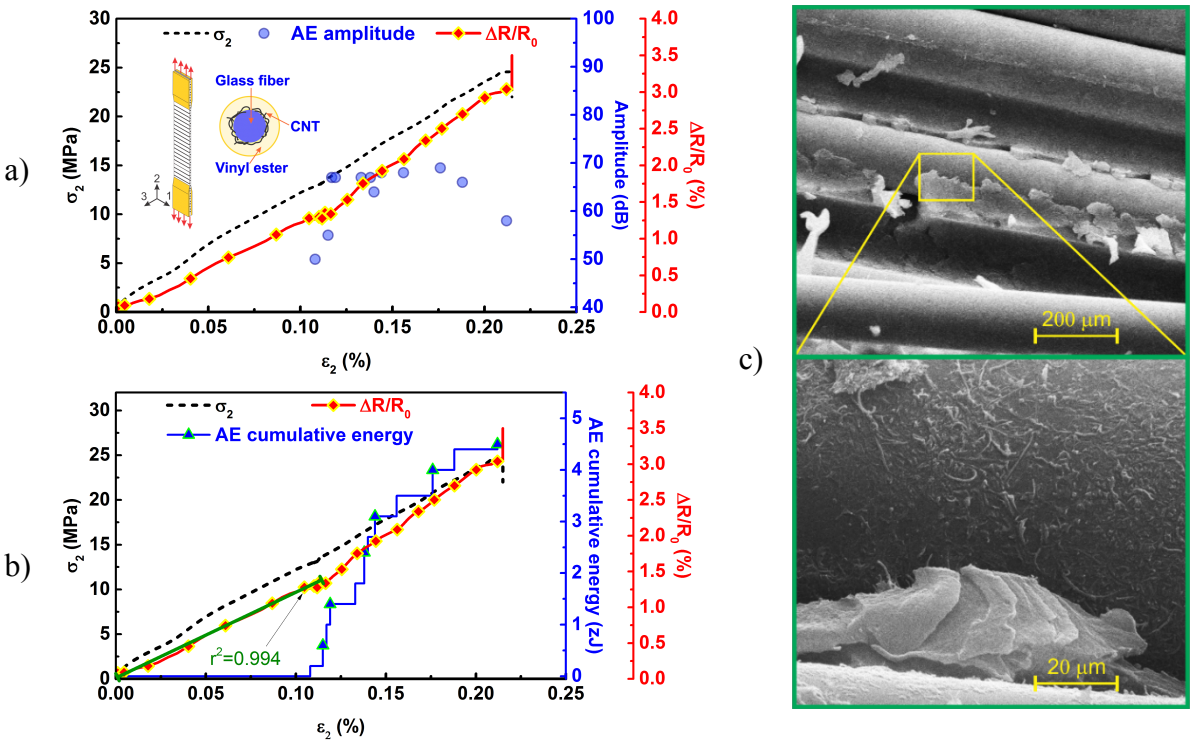

Figure 4. Mechanical, electromechanical, and acoustic emission characterization of the 90° composites with hierarchical architecture *f*. a) σ_2 (dashed line), evolution of $\Delta R/R_0$ (diamonds), AE amplitude (scattered circles), b) AE cumulative energy (triangles) as function of ε_2, c) SEM image of fractured surface.

3.2. *Damage sensing for 0° specimens*

The electrical sensitivity of the tailored multiscale composites to detect fiber-dominated failure was investigated by using specimens with the continuous glass fiber aligned along the loading direction (0° specimens). Representative mechanical (σ_1 vs. ε_1) and electromechanical ($\Delta R/R_0$ vs. ε_1) behaviors of the composites with hierarchical architecture *m*, coupled with the acoustic emission signals for the 0° specimens are shown in Fig. 5. Figure 5a shows the stress (σ_1), the electrical response ($\Delta R/R_0$) and the amplitude of the acoustic emissions as a function of the axial strain (ε_1) for the composite architecture *m*. Cumulative energy (in aJ=1x10^{-18} J) of acoustic signals as function of strain is shown in Fig. 5b. Fig. 5c (top) shows the fractured surface of the composite, and the MWCNTs protruding from the shattered matrix (Fig. 5c, bottom) highlight the success in obtaining the intended composite with architecture *m*. As seen from Fig. 5a,

acoustic events are not detected until $\varepsilon_1 \approx 0.2\%$; thereafter, a large number of acoustic events with amplitudes in the range of 40-100 dB are observed. In Fig. 5b, the progressive accumulation of energy of the acoustic events as function of the applied strain for $\varepsilon_1 > 0.2\%$ indicates damage progression of the composite until collapse. Analysis of the acoustic events show that composite damage is a combination of three major damage mechanisms, viz. matrix microcracking (40-60 dB), fiber/matrix debonding (60-70 dB), and fiber breakage (>70 dB) (Godin et al., 2004; Godin et al., 2005). For low levels of strain ($\varepsilon_1 < 0.2\%$) the lack of acoustic events (see Fig. 5a) suggests that the integrity of the composite is intact and hence, the changes the electromechanical response of this composite for $\varepsilon_1 < 0.2\%$ is ascribed to piezoresistivity. Such a piezoresistive response is originated from the deformation of the CNT network located within the matrix when is loaded, inducing changes in the electrical resistance at the macroscale. For $0.2\ \% \leq \varepsilon_1 \leq 1.0\ \%$, the main damage mechanism is ascribed to matrix cracking, as suggested by the large number of acoustic events with amplitudes of 40-60 dB. In addition to matrix cracking, some acoustic events associated to fiber/matrix debonding (60-70 dB) are also detected for $0.2\ \% \leq \varepsilon_1 \leq 1.0\ \%$. The increase in electrical resistance in this region ($0.2\ \% \leq \varepsilon_1 \leq 1.0\%$) exhibits some oscillations, which are attributed to the propagation of unstable cracks through the matrix, which destroy effective conductive pathways. This behavior is expected since, in this architecture, the MWCNTs are located within the matrix and any change in the initial network configuration produces a change in the electrical resistance of the composite. As seen in Fig. 5a, the number of acoustic events associated to fiber/matrix debonding progressively increase from $\varepsilon_1 \approx 1\ \%$ until specimen collapse. As indicated by the acoustic events with amplitudes >70 dB, fibers start breaking at $\varepsilon_1 \approx 1\ \%$ and this continues up to failure. For $\varepsilon_1 \geq 1.5\ \%$ the AE signal indicates that the events associated to fiber breakage have increased considerably in frequency. This is also observed in the micrograph of the fractured surface of the composite (Fig. 5c, top) where glass fibers exhibit brittle fracture. However, the $\Delta R/R_0$ signal does not properly capture such damage associate to fiber breakage, until imminent collapse; this is again due to the tailored location of the MWCNTs within the hierarchical composite, since in this architecture (*m*), the MWCNTs are allocated within the matrix (rather than on the fibers). Albeit its poor sensitivity to fiber breakage, the $\Delta R/R_0$ signal of composites with architecture *m* indirectly detects certain fiber breakage, likely because of matrix cracking at the vicinity of the broken fibers. Therefore, the

fact that the $\Delta R/R_0$ signal is sensitive to matrix cracking and fiber/matrix debonding but poorly sensitive to fiber breakage.

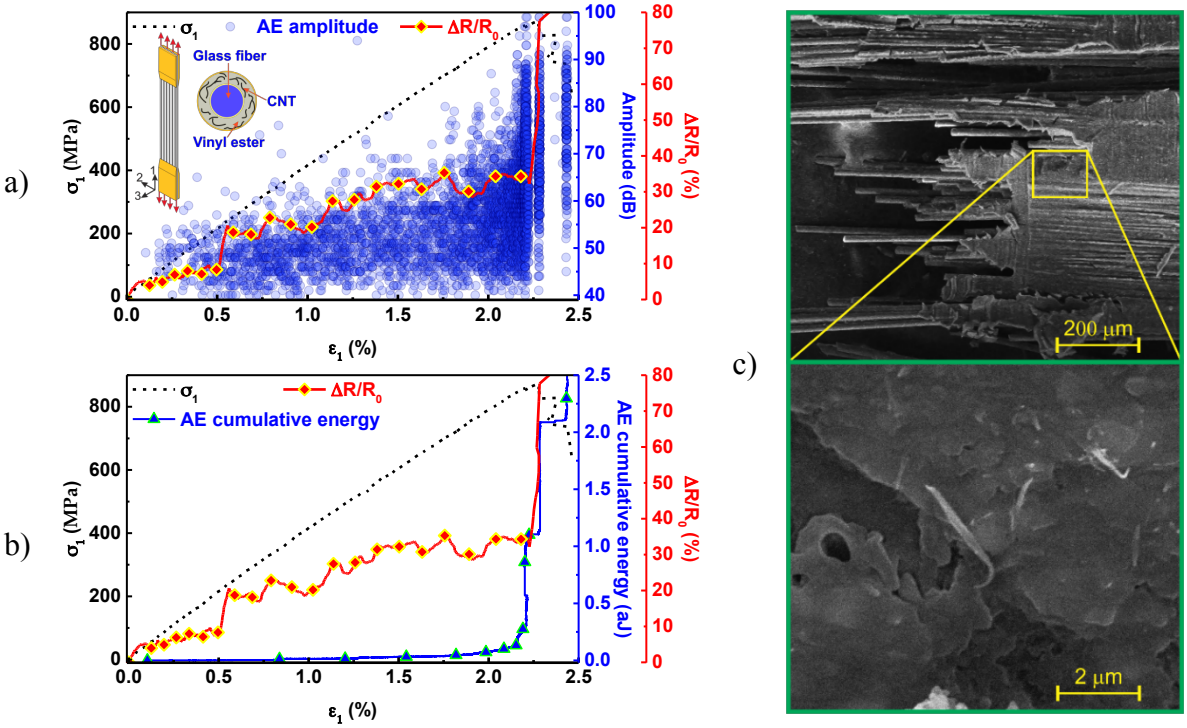

Figure 5. Mechanical, electromechanical, and acoustic emission signals of the 0° composites with hierarchical architecture *m*. a) σ_1 (dashed line), evolution of $\Delta R/R_0$ (diamonds), AE amplitude (scattered circles), b) AE cumulative energy (triangles) as function of ε_1, c) SEM of fractured surface.

Figure 6 shows the corresponding results for the 0° specimens with architecture *f*. For small deformations ($\varepsilon_1 \leq 0.2\%$), $\Delta R/R_0$ monotonically increases in a linear fashion. As mentioned above, acoustic events are not detected at such strain levels, supporting the fact that the changes in electrical resistance at such a low strain levels ($\varepsilon_1 < 0.2\%$) are due to piezoresistivity. For small deformations, the tensile strain applied to the composite equally stretches the matrix and fibers, which modifies the separation of the MWCNT network on the fibers, yielding an increase in $\Delta R/R_0$. For larger deformations ($\varepsilon_1 > 0.2\%$), acoustic events are detected suggesting the onset of composite damage, and the concomitant $\Delta R/R_0$ response increases monotonically following a nonlinear trend. The increase in the slope of the electromechanical signal is ascribed to the onset of irreversible phenomena (damage) occurring within the composite. For $0.2\% < \varepsilon_1 \leq 1.0\%$, damage within the composite is associated to matrix (40-60 dB) as well as to some fiber/matrix

debonding (60-70 dB), as seen from the acoustic events. It is likely that defects within the composites grow through the matrix and propagate towards the fiber/matrix interface. According to AE, fiber breakage occurs at $\varepsilon_1 > 1.0\%$, as suggested by the amplitudes >70 dB. For such strain levels, the $\Delta R/R_0$ response exhibits important increments, which accurately correlate with important changes in the cumulative energy of AE (Fig. 6b). In fact, the shape of the $\Delta R/R_0$ curve outstandingly follows that of the AE cumulative energy, as observed in Fig. 6b. Notice that at $\varepsilon_1 = 1.7$ % there is a prominent increase in $\Delta R/R_0$, which is associated to an increase in the occurrence of fiber breakage. It is assumed that when the fibers break at those strain levels, fiber breakage is accompanied by more damage within the composite in the form of matrix cracking and fiber/matrix debonding (see amplitudes of the acoustic events in Fig. 6a). Above $\varepsilon_1 = 1.7$ %, $\Delta R/R_0$ sharply increases indicating continues fiber breakage until $\varepsilon_1 = 2.0$ %, where an abrupt change in electrical resistance is observed, suggesting that a considerably number of fibers have been broken. However, the composite still maintains limited load bearing capacity, and the load is continuously redistributed as the fibers break until collapse of the specimen close to $\varepsilon_1 = 2.5\%$. The fractured surface of the composite with architecture *f* is similar to that of the composite with architecture *m,* where glass fibers exhibit brittle fracture. After fracture of this composite architecture, MWCNTs still remain deposited onto the fibers, as seen in Fig. 6c (bottom). In contrast to the composite with architecture *m* (Fig. 5), important variations in electrical resistance are observed when fiber breakage or fiber/matrix debonding occurs, since MWCNTs are deposited on the fibers. For the composite with architecture *f* subjected to tensile loading, glass fiber breakage and fiber/matrix debonding yield disruption of effective conductive pathways (located at the fiber/matrix interface region). This in turn induces large changes in the electrical resistance of the composite. Notice that the composite with architecture *f* (Fig. 6) exhibits a slightly lower tensile strength than that of the composite with architecture *m* (Fig. 5); this is likely a manufacturing issue related to fiber misalignment and additional manipulation during MWCNT deposition onto such MWCNT-modified fibers.

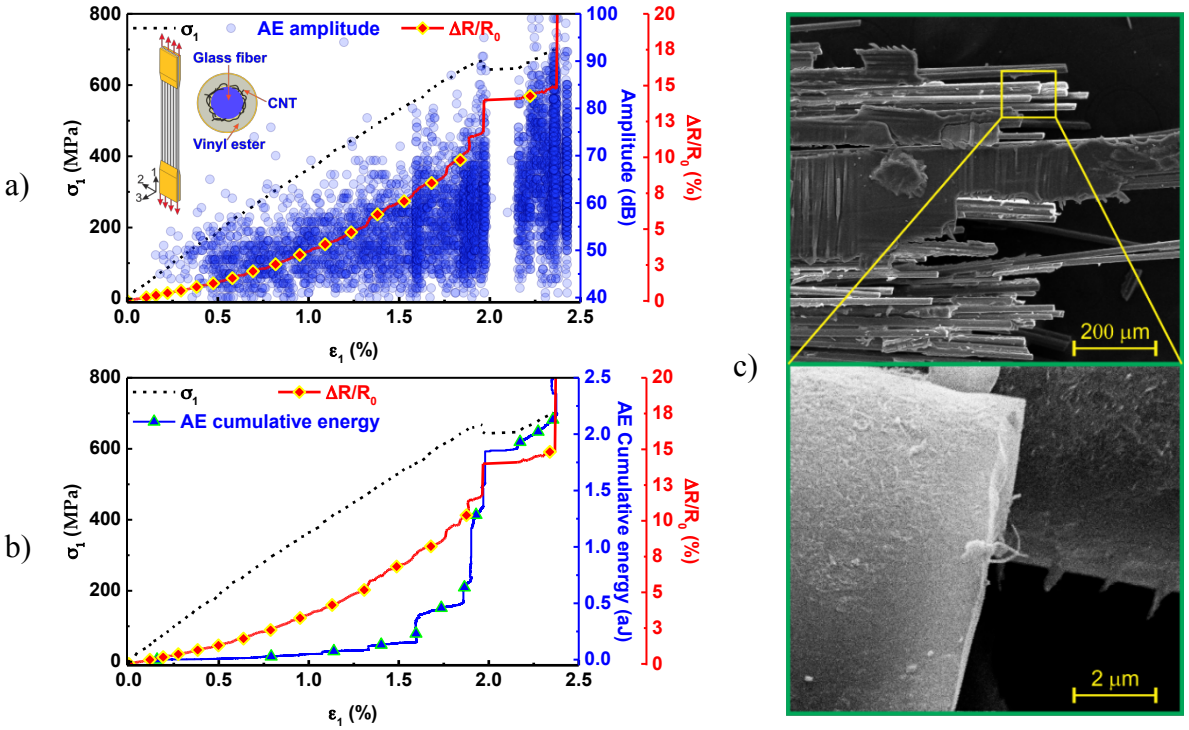

Figure 6. Mechanical, electromechanical, and acoustic emission signals of the 0° composites with hierarchical architecture *f*. a) σ_1 (dashed line), evolution of $\Delta R/R_0$ (diamonds), AE amplitude (scattered circles), b) AE cumulative energy (triangles) as function of ε_1, c) SEM image of fractured surface.

Conclusions

Multiscale hierarchical composites comprising glass fibers/multiwall carbon nanotube (MWCNT)/vinyl ester resin with tailored location of MWCNTs have been manufactured and characterized under coupled electromechanical testing and acoustic emissions. The MWCNT network was deliberatively placed either dispersed within the vinyl ester matrix (architecture *m*), or bonded to the glass fibers (architecture *f*), in order to examine the selectivity of the electrical signal (changes in electrical resistance) upon uniaxial loading. As a proof of concept and because of their known failure modes, unidirectional glass fiber/carbon nanotube/vinyl ester specimens with fibers oriented along (0°) and transverse (90°) to the loading direction were tested under uniaxial tension.

For composites with fibers oriented 90° with respect the loading direction, the onset of matrix cracking and fiber/matrix debonding were more accurately captured by the composites with MWCNTs deposited on the fibers. For composites with fibers oriented 0° with respect to the

loading direction, the composite architecture with MWCNTs dispersed within the matrix showed high electrical sensitivity to matrix cracking, but poor sensitivity to fiber and fiber/matrix interface damage. In general, the electrical response of the composites containing MWCNTs on the glass fibers showed more sensitivity to fiber failure and fiber/matrix debonding than the composites with MWNCTs dispersed into the matrix, but those composites with MWCNTs solely into the matrix were more sensitive to matrix microcracking. Therefore, both hierarchical composite architectures (*m* and *f*) are able to self-sense their own damage, and the location of the MWCNTs (on the fiber or within the matrix) renders increased selectivity for specific failure mechanisms. The multiscale hierarchical composites developed in this study are excellent candidates to be exploited for structural health monitoring applications, and their electrical sensitivity can be tailored for specificity from their hierarchical structure regarding the MWCNT location within the composite.

Acknowledgments

This work was supported by CONACYT grant number 220513 under the direction of Dr. FA. Support of the infrastructure acquired through CONACYT project No. 253762 is also appreciated. The authors thank MS. Marco Cen, Dr. Oscar Pacheco, Dr. Gustavo Dominguez and Dr. Alejandro May-Pat for their technical support, as well as Dr. Rolando Rios for the loan of the AE equipment.

References

An Q, Rider AN and Thostenson ET. (2013) Hierarchical Composite Structures Prepared by Electrophoretic Deposition of Carbon Nanotubes onto Glass Fibers. *ACS Applied Materials & Interfaces* 5: 2022-2032.

ASTM-International. (2011) D2584-11. Standard Test Method for Ignition Loss of Cured Reinforced Resins. West Conshohocken, PA: ASTM International.

ASTM-International. (2014) D3039-14. Test Method for Tensile Properties of Polymer Matrix Composite Materials. West Conshohocken, PA: ASTM International.

Ativitavas N, Fowler TJ and Pothisiri T. (2004) Identification of Fiber Breakage in Fiber Reinforced Plastic by Low-Amplitude Filtering of Acoustic Emission Data. *Journal of Nondestructive Evaluation* 23: 21-36.

Avilés F, Cauich-Rodríguez JV, Moo-Tah L, et al. (2009) Evaluation of Mild Acid Oxidation Treatments for MWCNT Functionalization. *Carbon* 47: 2970-2975.

Balageas D, Fritzen C-P and Güemes A. (2006) Structural Health Monitoring. Newport Beach: Wiley.

Chia Chen C, Jung-Ryul L and Hyung-Joon B. (2008) Structural Health Monitoring for a Wind Turbine System: a Review of Damage Detection Methods. *Measurement Science and Technology* 19: 122001.

Diamanti K and Soutis C. (2010) Structural Health Monitoring Techniques for Aircraft Composite Structures. *Progress in Aerospace Sciences* 46: 342-352.

Farrar CR and Worden K. (2007) An Introduction to Structural Health Monitoring. *Philosophical Transactions of the Royal Society A* 365: 303-315.

Fernberg P, Nilsson G and Joffe R. (2009) Piezoresistive Performance of Long-Fiber Composites with Carbon Nanotube Doped Matrix. *Journal of Intelligent Material Systems and Structures* 20: 1017-1023.

Friedrich SM, Wu AS, Thostenson ET, et al. (2011) Damage Mode Characterization of Mechanically Fastened Composite Joints Using Carbon Nanotube Networks. *Composites Part A: Applied Science and Manufacturing* 42: 2003-2009.

Gallo GJ and Thostenson ET. (2015) Electrical characterization and modeling of carbon nanotube and carbon fiber self-sensing composites for enhanced sensing of microcracks. *Materials Today Communications* 3: 17-26.

Gao L, Thostenson ET, Zhang Z, et al. (2009a) Coupled Carbon Nanotube Network and Acoustic Emission Monitoring for Sensing of Damage Development in Composites. *Carbon* 47: 1381-1388.

Gao L, Thostenson ET, Zhang Z, et al. (2009b) Sensing of Damage Mechanisms in Fiber-Reinforced Composites under Cyclic Loading using Carbon Nanotubes. *Advanced Functional Materials* 19: 123-130.

Gao S-l, Zhuang R-C, Zhang J, et al. (2010) Glass fibers with carbon nanotube networks as multifunctional sensors. *Advanced Functional Materials* 20: 1885-1893.

Godin N, Huguet S and Gaertner R. (2005) Integration of the Kohonen's Self-organising Map and k-means Algorithm for the Segmentation of the AE Data Collected During Tensile Tests on Cross-Ply Composites. *NDT & E International* 38: 299-309.

Godin N, Huguet S, Gaertner R, et al. (2004) Clustering of Acoustic Emission Signals Collected During Tensile Tests on Unidirectional Glass/Polyester Composite Using Supervised and Unsupervised Classifiers. *NDT&E International* 37: 253-264.

Hao B, Ma Q, Yang S, et al. (2016) Comparative study on monitoring structural damage in fiber-reinforced polymers using glass fibers with carbon nanotubes and graphene coating. *Composites Science and Technology* 129: 38-45.

Irving PE and Soutis C. (2014) Polymer Composites in the Aerospace Industry. Cambridge, UK: Woodhead Publishing.

Kostopoulos V, Vavouliotis A, Karapappas P, et al. (2009) Damage Monitoring of Carbon Fiber Reinforced Laminates Using Resistance Measurements. Improving Sensitivity Using Carbon Nanotube Doped Epoxy Matrix System. *Journal of Intelligent Material Systems and Structures* 20: 1025-1034.

Ku-Herrera JJ, Avilés F, Nistal A, et al. (2015) Interactions between the glass fiber coating and oxidized carbon nanotubes. *Applied Surface Science* 330: 383-392.

Ku-Herrera JJ, Avilés F and Seidel GD. (2013) Self-Sensing of Elastic Strain, Matrix yielding and Plasticity in Multiwall Carbon Nanotube/Vinyl Ester Composites. *Smart Mater Struct* 22: 085003.

Ku-Herrera JJ, Cauich-Rodríguez JV and Avilés F. (2014) On the role of fiber coating in the deposition of multiwall carbon nanotubes onto glass fibers. *Nanoscience and Nanotechnology Letters* 6: 932-935.

MacInnes D. (1992) Creating Conducting Materials Through Solution Blending of Conducting Polymers With Commercial Polymers. In: Salamone JC and Riffle JS (eds) *Contemporary Topics in Polymer Science.* Boston, MA: Springer, 380.

Marec A, Thomas JH and El Guerjouma R. (2008) Damage Characterization of Polymer-based Composite Materials: Multivariable analysis and Wavelet Transform for Clustering Acoustic Emission Data. *Mechanical Systems and Signal Processing* 22: 1441-1464.

Masmoudi S, Mahi AE, Turki S, et al. (2014) Mechanical Behavior and Health Monitoring by Acoustic Emission of Unidirectional and Cross-ply Laminates Integrated by Piezoelectric Implant. *Applied Acoustics* 86: 118-125.

Schulte K and Baron C. (1989) Load and Failure Analyses of CFRP Laminates by Means of Electrical Resistivity Measurements. *Composites Science and Technology* 36: 63-76.

Sebastian J, Schehl N, Bouchard M, et al. (2014) Health monitoring of structural composites with embedded carbon nanotube coated glass fiber sensors. *Carbon* 66: 191-200.

Thostenson ET and Chou T-W. (2008) Carbon Nanotube-based Health Monitoring of Mechanically Fastened Composite Joints. *Composites Science and Technology* 68: 2557-2561.

Wang X and Chung DDL. (1998) Self-monitoring of Fatigue Damage and Dynamic Strain in Carbon Fiber Polymer-Matrix Composite. *Composites Part B: Engineering* 29: 63-73.

Wang X, Fu X and Chung DDL. (1999) Strain Sensing Using Carbon Fiber. *Journal of Materials Research* 14: 790-802.

Wiegand N and Mäder E. (2016) Multifunctional Interphases: Percolation Behavior, Interphase Modification, and Electro-Mechanical Response of Carbon Nanotubes in Glass Fiber Polypropylene Composites *Advanced Engineering Materials* 18: 376-384.

Xiaojun W and Chung DDL. (1996) Continuous Carbon Fibre Epoxy-matrix Composite as a Sensor of its Own Strain. *Smart Materials and Structures* 5: 796.

Xiaojun W and Chung DDL. (1997) Real-time Monitoring of Fatigue Damage and Dynamic Strain in Carbon Fiber Polymer-matrix Composite by Electrical Resistance Measurement. *Smart Materials and Structures* 6: 504.

Zhang H, Bilotti E and Peijs T. (2015a) The use of carbon nanotubes for damage sensing and structural health monitoring in laminated composites: a review. *Nanocomposites* 1: 167-184.

Zhang H, Kuwata M, Bilotti E, et al. (2015b) Integrated Damage Sensing in Fibre-Reinforced Composites with Extremely Low Carbon Nanotube Loadings. *Journal of Nanomaterials* 2015: 7.

Zhang J, Zhuang R, Liu J, et al. (2010) Functional interphases with multi-walled carbon nanotubes in glass fibre/epoxy composites. *Carbon* 48: 2273-2281.